JOURNAL OF GEOPHYSICAL RESEARCH, VOL. 105, NO. C1, PAGES 1209–1225, JANUARY 15, 2000

Modeling the impact of fronts and mesoscale circulation on the nutrient supply and biogeochemistry of the upper ocean

Amala Mahadevan[1] and David Archer
Department of Geophysical Sciences, University of Chicago, Chicago, Illinois

Abstract. A new model for three-dimensional mesoscale flow is used to simulate the vertical transport of nutrients into the euphotic zone from deeper waters. We use the model to diagnose the effects of mesoscale motions on the upper ocean biogeochemical cycles of NO_3, CO_2, O_2, sea surface exposure tracers that resemble dissolved organic carbon (DOC) and H_2O_2, and the corresponding rates of new production and gas exchange in regions near the Joint Global Ocean Flux Study (JGOFS) oligotrophic time series sites of Hawaii and Bermuda during late summer. The physical model is nonhydrostatic and designed to handle open boundaries without excessive damping as described by *Mahadevan and Archer* [1998]. It is initialized and driven at the open boundaries with flow fields from the 1/4° global circulation model of *Semtner and Chervin* [1992]. We examine the effect of model resolution and the attending increase in mesoscale and frontal-scale motions on the nutrient and carbon chemistry of the upper ocean. New production, approximated and diagnosed as an exponential uptake of nutrients within the euphotic zone, increases with model resolution. Nutrient is supplied for new production where isopycnals from the subsurface outcrop at the base of the euphotic zone, primarily at fronts. The rate and spatial scale of upwelling and nutrient uptake are more sensitive to model resolution than are temperature or the more slowly responding geochemical tracers such as CO_2.

1. Introduction

The chemistry of the upper ocean and the interaction of the ocean with atmospheric CO_2 are intimately controlled by the pattern of flow and mixing in near surface waters. Photosynthesis in sunlit surface waters fixes dissolved CO_2 into particulate and dissolved organic carbon (DOC). Some of this carbon is exported into the deep by sinking or by entrainment with downwelling water. In oligotrophic subtropical waters the rate of particulate organic carbon and DOC export, which equals the rate of new (nonregenerative) production in the steady state, is limited by the availability of macronutrients NO_3 and PO_4. The export of nutrients from the euphotic zone in the form of dissolved nitrogen and particulate organic nitrogen in sinking organic matter must be replenished to maintain the level of production in surface waters.

Measurements of oxygen concentrations at the sea surface have provided a new means for estimating net carbon export production [*Spitzer and Jenkins*, 1989] that does not rely on the trapping of sinking particulate organic matter. Net photosynthesis leaves behind relict oxygen, which either mixes to deeper waters, remains within a supersaturated oxygen maximum zone below the mixed layer until it is ventilated by winter mixing, or evaporates to the atmosphere. The rate of oxygen degassing, which is an indicator of the minimum rate of new production, can be calculated from oxygen supersaturation measurements of surface waters using the kinetics of gas exchange (after correction for temperature-related solubility changes and bubble entrainment). Such measurements [*Emerson et al.*, 1991, 1997] document high rates of carbon export production in the subtropical gyres (~2.7 moles carbon m^{-2} yr^{-1}). A helium budget for surface waters [*Jenkins*, 1988] near Bermuda suggests considerable vertical exchange of subsurface waters with the euphotic zone, also supporting a higher new production rate in agreement with the oxygen-based estimates. Other methods for estimating net carbon export include short-term changes in the oxygen anomaly and nitrogen concentrations [*Michaels et al.*, 1994b], carbon isotopic budgets [*Quay and Anderson*, 1996], isotopically labeled ni-

[1]Now at Atmospheric and Environmental Research, Cambridge, Massachusetts.

Paper number 1999JC900216.
0148-0227/00/1999JC900216$09.00

trogen uptake [*Emerson and Hayward*, 1995], tritium-based estimates of oxygen utilization rates [*Sarmiento et al.*, 1990], and remote sensing [*Sathyendranath et al.*, 1991]. Measurements of new production based on the export of particulate organic carbon [*Karl et al.*, 1996; *Lohrenz*, 1992; *Altabet*, 1989] can differ somewhat from oxygen- and tracer-based measurements, both due to certain limitations of sediment traps [*Michaels et al.*, 1994; *Buesseler*, 1991] such as grazing, solubilization of particulate matter, and hydrodynamic overtrapping or undertrapping, and the fact that export of organic carbon in dissolved form can be significant at times [*Carlson et al.*, 1994]. Hence the nonparticulate methods of estimating new production can be considered more reliable and representative of the total organic carbon (TOC) exported from from the euphotic zone, rather than merely the particulate organic carbon. These various measurements suggest that rates of carbon export production within the subtropical gyres are in the range of 2–4 moles carbon m^{-2} yr^{-1}, much higher than estimated earlier [*Eppley and Peterson*, 1979]. The implication of these higher modern estimates of carbon export in the oligotrophic oceans is that the vast subtropical gyres are far more productive than envisioned and contribute significantly to the global biological organic carbon pump.

In oligotrophic waters such as those sampled by the Joint Global Ocean Flux Study (JGOFS) Hawaii Oligotrophic Time-series (HOT) and Bermuda Atlantic Time-series Study (BATS) stations the mechanism for the replenishment of nutrients in the surface waters is not obvious. The diurnal and seasonal deepening and shoaling of the mixed layer explain the abundance of phytoplankton in the spring time but do not explain the continued production that is observed in the late summer. The thermocline maximum in nutrient concentration is maintained by decomposition of organic matter sinking from above, thereby depleting sea surface concentrations. The simplest potential source of dissolved nutrients is this nutrient-rich subsurface water, but the means by which it is brought to the surface remained somewhat of a mystery. Turbulence within the thermocline mixes substances irreversibly across the density stratification, but typical rates of mixing of 0.1 cm^2 s^{-1} (inferred from microstructure temperature or velocity fluctuations [*Caldwell*, 1983] and measurements of the spreading of an artificially introduced tracer in the thermocline [*Ledwell et al.*, 1993]), acting on observed nutrient-depth profiles in this region, result in a nutrient flux that is an order of magnitude smaller than that inferred from tracer estimates of new production. Estimates of nutrient fluxes based on fine-scale turbulent kinetic energy measurements and nutrient profiles in the upper ocean [*Lewis et al.*, 1986] also underpredict new production by a factor of 3–4.

Large-scale upwelling or the Ekman flux resulting from wind divergence is only of the order of 50–100 m yr^{-1} and makes no contribution in the subtropical gyres where the net flux is downward. Much of the diapycnal mixing in the ocean may occur at boundaries, but the depleted surface concentration precludes much horizontal transport of nutrient to oligotrophic waters in surface currents. The oceanographic observation is that surface waters are entirely depleted of dissolved inorganic nutrients throughout large regions of the subtropical gyre for most or all of the annual cycle. Three-dimensional ocean circulation models with biogeochemistry [*Najjar*, 1990; *Bacastow and Maier-Reimer*, 1991; *Najjar et al.*, 1992; *Maier-Reimer*, 1993; *Sarmiento et al.*, 1993] tend to underpredict rates of carbon export production in oligotrophic waters unless sea surface nutrient concentrations are elevated unrealistically, or nutrients in dissolved organic form are thought to be significant, thus allowing horizontal transport of nutrients in surface currents from equatorial and coastal upwelling zones [*Williams and Follows*, 1998]. This suggests that though the coarse-resolution global circulation models are able to resolve large-scale horizontal flow, there is some mechanism for nutrient transport to the oligotrophic euphotic zone that is missing from them.

The magnitude of vertical exchange between subsurface and surface waters inferred from the ^3He degassing rate [*Jenkins*, 1988] is sufficient to account for the observed levels of production. This implies that even though other biological or chemical mechanisms for nutrient supply, such as the active transport of nutrients by diatoms and nitrogen fixation in stratified waters, may make a contribution, the physical transport of subsurface water facilitates a major part of the nutrient replenishment to the surface. Nutrients can also remain concealed in the form of dissolved organic matter (DOM), but DOM generally contains reduced carbon that would be released and oxidized if the dissolved nutrients (dissolved organic nitrogen) were consumed. Hence the supply of nutrients through DOM would not support the same high observed rate of oxygen degassing to the atmosphere. Other mechanisms such as atmospheric deposition are thought to make little contribution to the supply of the nitrate and phosphate in the subtropical gyres and are neglected in this study.

Several observations suggest that mesoscale eddies and fronts (regions of high horizontal gradients in water density) play a significant role in vertical transport and in the supply of nutrients to the euphotic zone. A significant portion of the ocean's kinetic energy resides in the mesoscale (10–100 km length), characterized by the Rossby radius of deformation, a length scale at which the Coriolis and hydrostatic pressure gradient forces come into balance. Eddies typically equilibrate in features of this size and exhibit a doming of isopycnals or a circular front-like structure. Fronts are also continually generated in surface waters by the stretching and deformation of the evolving flow field. They are characterized by an even smaller length scale (typically

~10 km) in the across-gradient direction. Frontogenesis theories [*Hoskins and Bretherton*, 1972], observations of ocean fronts [*Pollard and Regier*, 1990] and eddies [*Rudnick*, 1996; *Shearman et al.*, 1999], and models of frontogenesis [*Bleck et al.*, 1988; *Spall*, 1995] indicate that the vertical velocities in fronts are orders of magnitude larger than the vertical velocity due to Ekman pumping. Frontal regions, where isopycnals rise sharply to the surface, and the enhanced vertical transport that takes place within them are not captured by the resolution that is typically afforded in large-scale circulation models.

The role of eddies in pumping nutrients to the surface has recently been identified as the dominant nutrient supply mechanism in the Sargasso Sea [*McGillicuddy et al.*, 1998]. In a modeling study, *McGillicuddy and Robinson* [1997] characterize the effect of eddies on biological new production by driving a quasigeostrophic model with a periodic artificial eddy field made up of the most dominant modes observed in the Mid-Ocean Dynamics Experiment (MODE) data near Bermuda. Their nutrient model test bed is a subregion in the interior of their domain where nonlinearities make the flow develop into what it may look like in the real ocean. They simulate perpetual summer for several hundred days and achieve rates of biological production in close agreement with observed values of 50 g carbon m^{-2} yr^{-1}. The strength of eddy pumping and estimated rate of nutrient transport differ, however, from nutrient supply rates of *Oschlies and Garcon* [1998] and earlier attempted measurements of eddy pumping rates by *Falkowski et al.* [1991].

In this study we attempt to characterize the effect of frontal and mesoscale features on the nutrient cycles at the JGOFS stations in the subtropical gyres. We use a new high-resolution three-dimensional model to simulate a region of the subtropical gyre and to observe the effect of increasingly smaller scales on the vertical transport of nutrients across the base of the euphotic zone and the biogeochemistry of the surface waters. We use initial and time-varying open boundary conditions taken from the 1/4° global circulation model of *Semtner and Chervin* [1992] (hereafter SC). Nutrient concentrations are initialized using an artificial nutrient-density relationship that produces a nutrient-depth profile similar to that observed in the region. We simulate nonregenerative biological activity by a Newtonian restoration of nutrient to zero concentration within the euphotic zone. Initial and lateral boundary conditions on the euphotic zone are such that the simulated new production is entirely due to the vertical flux of nutrient from beneath the euphotic zone. We present late summer simulations near both JGOFS oligotrophic time series stations, Hawaii (HOT) and Bermuda (BATS).

Since our model is initialized and driven at the boundaries with the SC model output, the flow field in our model domain is largely dependent on it. The SC model flow fields have been tested by detailed comparison with with TOPEX/Poseidon sea surface height data and drifters [*McClean and Semtner*, 1997; *Stammer et al.*, 1996]. They are found to underrepresent the variability and eddy kinetic energy of the interior ocean but are otherwise quite realistic. In spite of a few shortcomings in the SC flow fields a regional model driven by them can serve very well as a tool to study the processes and understand the mechanisms of nutrient transport.

One aim of this paper is to assess the effect of mesoscale and frontal processes on the transport of nutrients and on the geochemical cycles of the upper ocean by using a range of model resolutions but identical initial and forcing conditions. A second goal is to search for geochemical signatures of mesoscale motions that might be detectable in the field. We examine the statistics of the chemical properties in the surface ocean and the dependence of biological production and its geochemical signatures on the density and structure of the flow.

Besides nutrient supply an enhanced vertical exchange between the surface and subsurface ocean also has implications on the exchange of heat and salt fluxes, tracers, and gases such as CO_2. While fossil fuel CO_2 will ultimately find its way into the deep oceans, the rate of CO_2 invasion into the thermocline is limited by the stratification of surface waters. Increased vertical exchange by mesoscale and frontal motions, however, implies greater mixing across the thermocline that allows more fossil fuel CO_2 laden surface water to mix down into the deep sea. Surface waters tend to have higher concentrations of DOC than do subsurface waters, implying that some component of DOC is generated and lost quickly relative to the timescale of mixing with subsurface waters. Enhanced exchange of surface water with subsurface waters by mesoscale motions will increase our estimates of the rate of DOC export from the euphotic zone.

2. Modeling

We use a three-dimensional nonhydrostatic model to simulate the mesoscale flow field in a limited region of the open ocean. The fluid dynamical model is particularly suited to modeling a region with open boundaries without the use of eddy viscosity or damping at the boundaries. For details on the model, boundary condition implementation and a discussion on the limitations of using such a model in a limited region, see *Mahadevan and Archer*, 1998. The model equations are solved numerically using a finite volume approach. The model domain, defined by four vertical boundary faces, the sea surface and the ocean bed is initialized and driven at the lateral boundaries using the 0.4° (This is better known as the 1/4° SC model as the globally averaged resolution of the Mercator grid is 1/4°. In the regions that we model the longitudinal and latitudinal resolution are 0.4° and 0.33°, respectively.) resolution flow fields from the global circulation model of SC which we interpolate in time and space onto our grid.

The horizontal grid is defined by lines of latitude and longitude. We use a resolution of 0.4° (as in SC) and, subsequently, increase it to 0.2° and 0.1°. In each case the 0.4° boundary and initial conditions are interpolated onto the grid used by the model. We are thus able to model the region at higher resolution than the model that provides the initial and boundary conditions. In the vertical we use an exponentially stretched grid with a total a 24 grid cells. The topmost layer of grid cells forms the mixed layer. Its depth is varied between 10 and 125 m by the bulk mixed layer model of *Chen and Rothstein* [1994]. The thermocline is finely discretized by eight layers up to a depth of 510 m. The midsection of the grid has horizontal surfaces, while the bottommost five layers are draped over the seafloor to conform to the topography. The grid spacing increases smoothly within each section and also from the surface to the bottom. As the mixed layer depth changes, water flows across the mixed layer boundary, and the thermocline section of the grid reconfigures itself to the new specification. The model also allows for convective adjustment once every several time steps. Since we find the model results to be more sensitive to horizontal rather than vertical refinement, we use the same vertical grid structure for all the different horizontal resolution cases described here.

We use the *Hellerman and Rosenstein* [1983] climatological monthly wind forcing and restore the surface temperature and salinity fields to monthly climatological *Levitus* [1982] data using a time constant of 1 month as is done in the SC model. The time step used for the model simulations presented here is 50 min.

We deploy the model in two 10° × 10° regions of the pelagic subtropical gyre: (1) 30°–40°N, 50°–60°W, in the vicinity of the BATS site, and (2) 10°–20°N, 140°–150°W, in the vicinity of the HOT site. At each of these sites we simulate the postsummer 120 day period from August through November, when the mixed layer is generally at its shallowest and any nutrients made available through seasonal mixed layer changes are already depleted from the euphotic zone. For each of the regions, initial and boundary conditions are extracted from the SC model fields corresponding to the same period and arbitrarily chosen from the year 1987. (The SC model was driven with smoothed European Centre for Medium-Range Weather Forecasts (ECMWF) monthly wind stresses for the period 1985–1989.) Although it would be nice to run the model for a period of several years in order to investigate long-term balances and seasonal phenomena such as the observed dissolved inorganic carbon (DIC) drawdown at Bermuda [*Michaels et al.*, 1994a], we are limited in the length of model simulations we can perform in a regional domain with boundary conditions prescribed from another model [*Mahadevan and Archer*, 1998].

Along with the fluid dynamical equations we model the distribution of nitrate and its uptake in the euphotic zone. In the oligotrophic ocean we may safely assume that the nutrient fluxed vertically into the euphotic zone is consumed by phytoplankton. The nutrient, denoted by N, is advected in a conservative manner everywhere, except in the euphotic zone, where it is consumed by biology. We model the nutrient consumption to occur at an exponential rate with an e-folding timescale of 2 weeks. Hence

$$\frac{DN}{Dt} = -\alpha_N N, \tag{1}$$

where

$$\alpha_N = 0 \tag{2}$$

beneath the euphotic zone, and

$$\alpha_N = (14 \text{ days})^{-1} \tag{3}$$

in the euphotic zone. Here

$$\frac{D}{Dt} \equiv \frac{\partial}{\partial t} + \mathbf{u} \cdot \nabla$$

is the material derivative, and $\mathbf{u}$ is the fluid velocity. Nitrate uptake or biological production is simulated in grid cells that lie within (or partly within) the euphotic zone.

Nitrate is taken to be the limiting nutrient in both locations and is used to limit production in the model. The nutrient concentrations are initialized as constant values on density surfaces using a nutrient-density relationship that reproduces the nutrient-depth distribution from the HOT and BATS data sets (Figure 1). Nutrient levels are observed to be fairly constant along isopycnals, but simply using the Levitus nutrient-density relationship to initialize the model results in a deeper nutricline than is observed at either the BATS or HOT locations. This is because the density in the upper layers of the SC model is lower than is observed at the BATS and HOT sites. At Bermuda the isopycnal spacing in the upper 400 m of the SC model fields is greater than in observations (see Figure 1). This results in our initial model nutrient values being lower than the data at a depth of 100–200 m. In order to contend with a more gradual increase of nutrient with depth in the model as compared to the data at BATS, we set the model's euphotic zone to be 160 m deep at Bermuda and 100 m deep at Hawaii.

Within the euphotic zone the nutrient concentration is initialized to zero. Water flowing horizontally into the euphotic zone through the boundaries is also specified to have zero nutrient concentration so that the diagnosed rate of production is supported entirely by vertical nutrient fluxes. An eddy diffusivity term and convective mixing are omitted so that the vertical nutrient fluxes are mimicked as advective. Nitrate uptake is converted into new production of carbon using a Redfield ratio (which specifies the molar proportions in which the constituent elements are found to occur in biological matter as well as in ocean water) C:N of 8:1 [*Takahashi et al.*, 1985]. Beneath the euphotic zone,

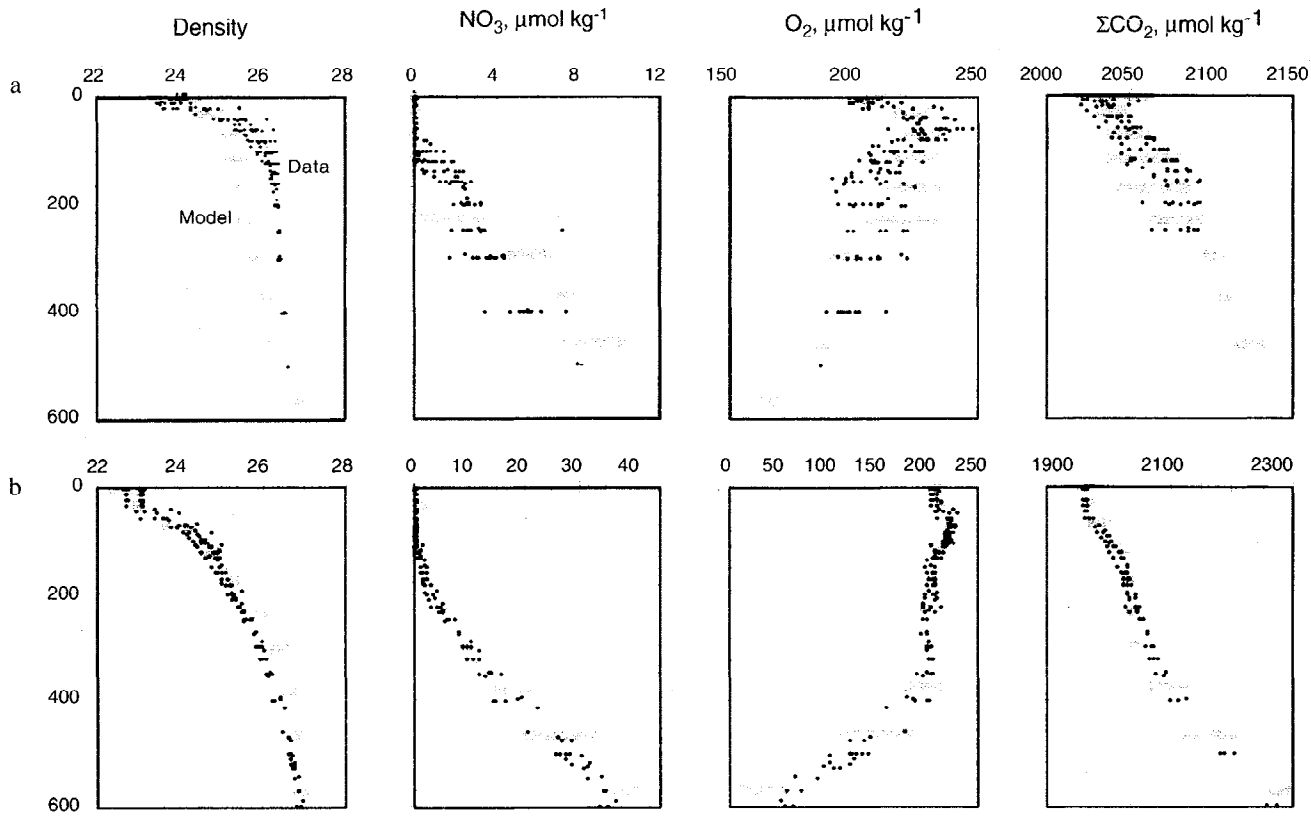

Figure 1. The range of initial fields of density, nitrate, oxygen, and total CO_2 used in the model at (a) Bermuda and (b) Hawaii are plotted as a function of depth (shaded bars) alongside measurements of these fields at the Hawaii Oligotrophic Time-series (HOT) and Bermuda Atlantic Time-series Study (BATS) sites (solid circles), respectively. The initial density distribution in the model (interpolated from the *Semtner and Chervin* [1992] (SC) model field) does not match the data very well, particularly near Bermuda. Hence we generate a nutrient-density relationship that reproduces the nutrient-depth profile at BATS and HOT, rather than use the Levitus nutrient-density relationship. Oxygen and total CO_2 are initialized using the Redfield ratios (-176:140:16 NO_3).

nutrient is resupplied to the water by the redissolution of sinking organic matter. The downward flux of sinking organic matter is modeled as decreasing (on account of remineralization) with depth by a power law as suggested by sediment trap measurements [*Martin et al.*, 1987]. The nitrate content of the sinking matter is given by

$$N_s(z) = N_s(z_e)\ (z/z_e)^{-0.8}, \qquad (4)$$

where N_s is the sinking flux of nitrate (in moles m^{-2} s^{-1}), z is the depth, and z_e is the euphotic horizon depth (set as 100 m). The difference in the sinking flux between two levels contributes a source of nutrient to the layer between.

Other biological tracers, O_2, total CO_2, alkalinity, and pCO_2, are coupled to NO_3 for their biological sources and sinks. Biological production occurs with CO_2 uptake and O_2 production, while remineralization is with O_2 uptake and CO_2 release. O_2 and CO_2 stoiciometries are modified Redfield ratios (-176:140:16 NO_3) [*Takahashi et al.*, 1985]. Alkalinity is conserved and only advected. It is used to calculate pCO_2. At the sea surface we compute the concentration of carbonic acid and the surface saturation state of CO_2 from alkalinity, total CO_2, temperature, and salinity using the Henry's law constant. The dissociation constants for carbonic acid and borate are taken from *Mehrbach et al.* [1973] and *Lyman* [1956], respectively. We let gas exchange adjust O_2 and CO_2 toward atmospheric saturation with a constant piston velocity of 3 m day^{-1}. The atmospheric flux is computed as the exchange coefficient (piston velocity) times the difference in concentration between the surface and saturation partial pressure. Initial distributions of O_2 and CO_2 are coupled to NO_3 and resemble their observed vertical distributions at BATS and HOT as seen in Figure 1.

Two other idealized sea surface exposure tracers are also modeled following the development of *Archer et al.* [1997]. The tracers are normalized to a 0–1 range using

$$c = (C - C_{\mathrm{deep}})/(C_{\mathrm{olig.surf.}} - C_{\mathrm{deep}}), \qquad (5)$$

where C is the tracer concentration. The normalized tracer c ranges from 0 in the deep ocean to 1 at the ex-

posed surface. The value of c is maintained by a depth-dependent production rate $P_{\max}\exp(-z/z_e)$, where z_e, the euphotic zone depth, is taken to be 100 m. The depletion of c is modeled as first-order depth-independent decay λc, where λ is a decay constant in units of inverse time. Since in the steady state we would desire a value of $c = 1$ be maintained at the surface (z=0) we set the production equal to decay so that

$$P_{\max} = \lambda = \tau_c^{-1}, \tag{6}$$

where τ_c is the timescale of both production and consumption. Hence, in the absence of flow,

$$\partial c/\partial t = \tau_c^{-1}(e^{-z/z_e} - c), \tag{7}$$

and the steady state scaled tracer concentration is given by

$$c_s = \exp(-z/z_e). \tag{8}$$

It ranges from 1 at the sea surface to 0 at depth with a scale depth of z_e, and deviations from this steady state profile are restored by exponential relaxation with timescale τ_c. To model this tracer in the flow field, we use

$$\frac{Dc}{Dt} = \tau_c^{-1}(e^{-z/z_e} - c), \tag{9}$$

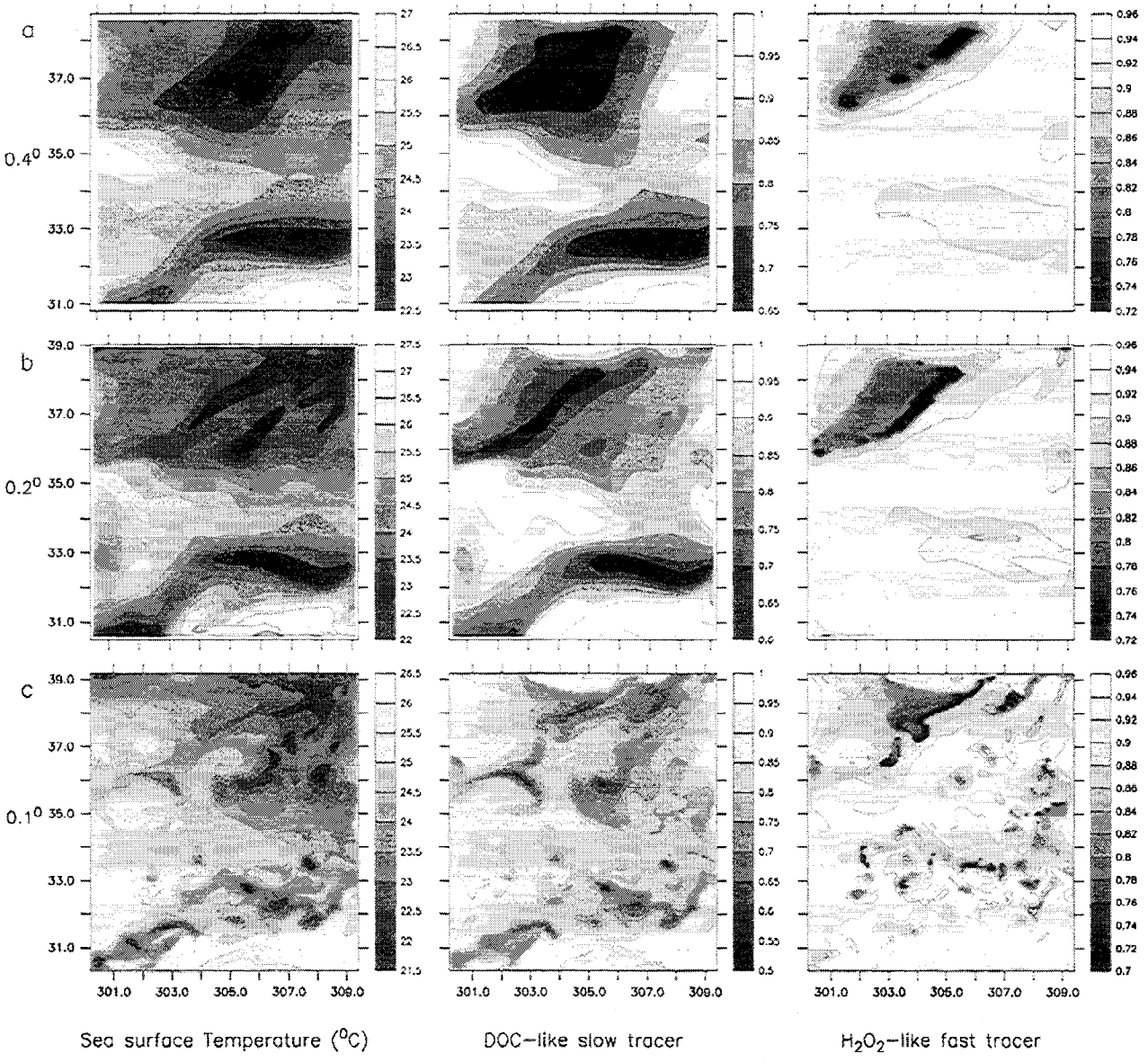

Figure 2a. A snapshot of the surface ocean near Bermuda on day 75 of the simulation. In each column, we show results from the (a) 0.4°, (b) 0.2° and (c) 0.1° models. The vertical grid in all our model runs is the same. The initial and boundary conditions for all model runs were interpolated from the SC flow fields. The sea surface properties plotted are temperature (°C), dissolved organic carbon (DOC)-like (slow) tracer (normalized 0–1), and H_2O_2-like fast tracer (normalized 0–1).

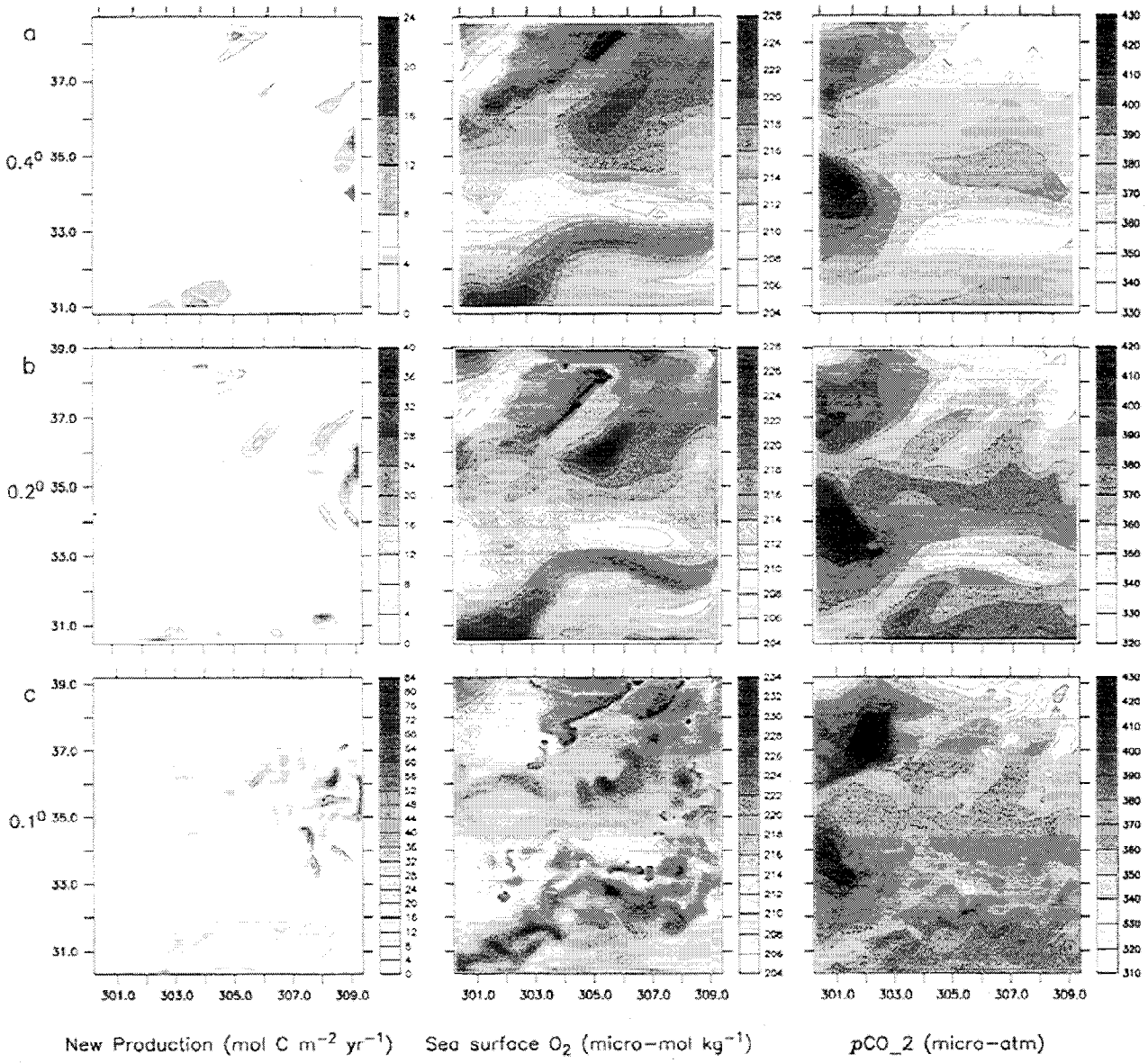

Figure 2b. Same as Figure 2a but for new production (moles carbon $m^{-2}yr^{-1}$), O_2 (μmol kg^{-1}), and pCO_2 (μatm).

where Dc/Dt is the material derivative, and allow the tracer concentration to evolve in the flow.

Two implementations of the ventilation tracer are run with timescales τ_c of 60 and 3 days, respectively. The slower recovering tracer is thought to simulate the sea surface excess of DOC concentration as in the equatorial Pacific Ocean [*Archer et al.*, 1997]. The faster tracer is intended to capture some of the behavior of hydrogen peroxide (H_2O_2) [*Johnson et al.*, 1989], which is produced photochemically in surface waters on something like a 3 day timescale.

3. Results

3.1. Effects of Mesoscale Motion on Upper Ocean Geochemistry

In our simulations, the ocean is transformed dramatically from relatively featureless at 0.4° and 0.2° resolution, to active and eddy-filled at 0.1° resolution. This can be seen in the sea surface temperature (SST) field plotted at different resolutions in Figures 2 and 3. In the regions modeled the internal Rossby radius is 40–60 km. It gets resolved only when the grid spacing is

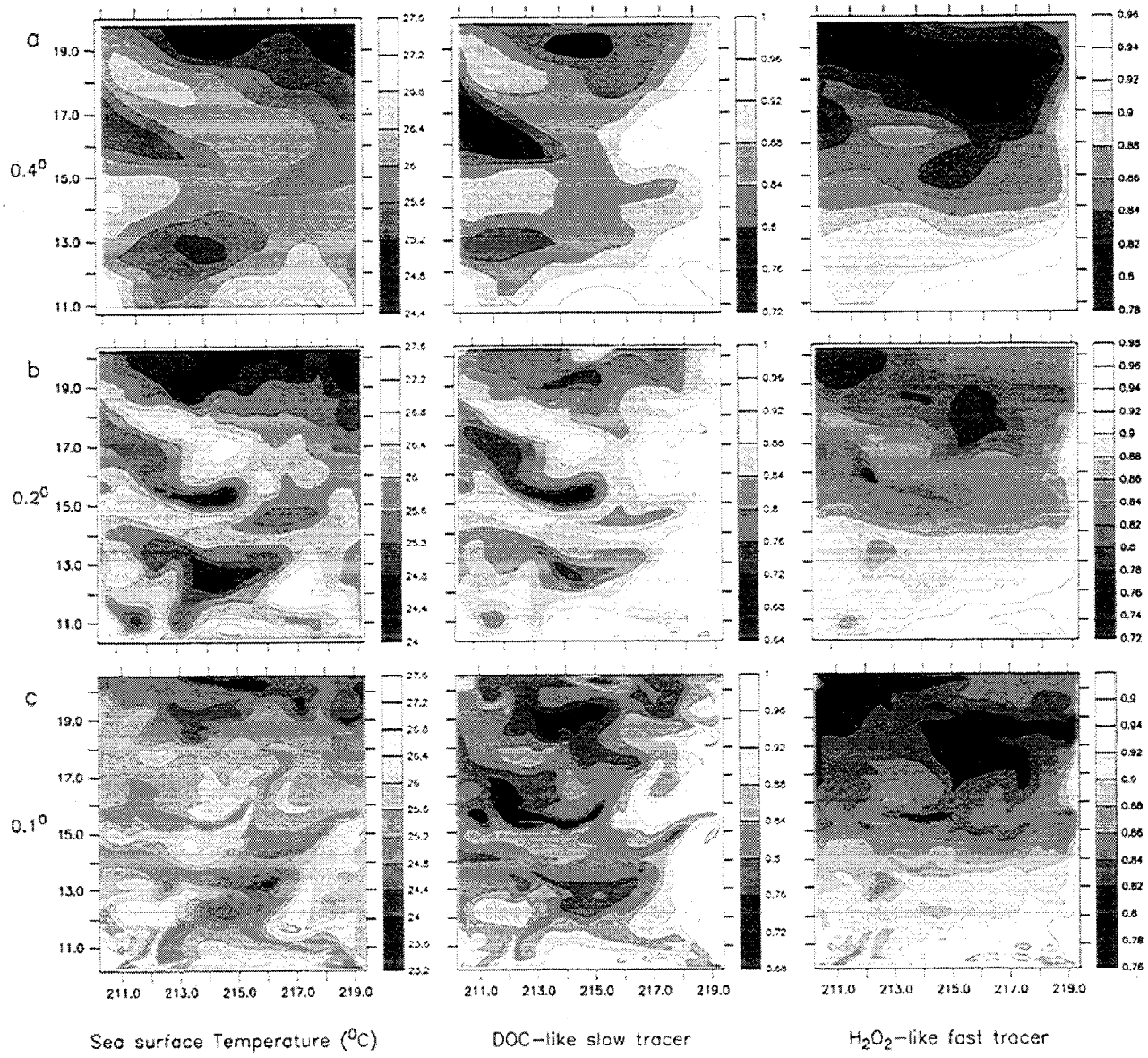

Figure 3a. A snapshot of the surface ocean near Hawaii on day 75 of the simulation. In each column, we show results from the (a) 0.4°, (b) 0.2°, and (c) 0.1° models. The vertical grid in all our model runs is the same. The initial and boundary conditions for all model runs were interpolated from the SC flow fields. The sea surface properties plotted are temperature (°C), DOC-like (slow) tracer (normalized 0–1), and H_2O_2-like fast tracer (normalized 0–1).

$\sim$ 0.1° or less, since at least four grid points are required to resolve a wavelength. The effect of increasing resolution on the temperature and tracer distributions is greatest when crossing the threshold at which the internal Rossby radius can manifest itself. In the future we would like to use yet higher resolution to confirm this, but for now we believe that the effect of further grid refinement would not be as dramatic as the transition from 0.2° to 0.1°.

Increasing model resolution greatly enhances vertical transport and nutrient uptake in the simple biological model. In Figure 4 we plot the rate of new production (averaged over the area of the model domain) inferred from the rate of nutrient uptake in the euphotic zone for different model resolutions. The simulations show increased biological activity at higher resolution on account of an increased supply of nutrient. The 0.1°-resolution model estimates a new production rate that is much closer to observations (see Table 1) than the 0.4° and 0.2° models in which the production is too low on account of the unresolved frontal and mesoscale transport mechanisms. Near Bermuda our 0.1°-resolution model predicts new production to be in the range of 2.2–3.6 moles carbon m^{-2} yr^{-1} in the post summer, generally a period of low productivity. Recent studies based on oxygen utilization rates [*Platt and Harrison*, 1985], oxygen cycling, and ^{3}He [*Jenkins and Goldman*, 1985] estimate new production to be in the range of

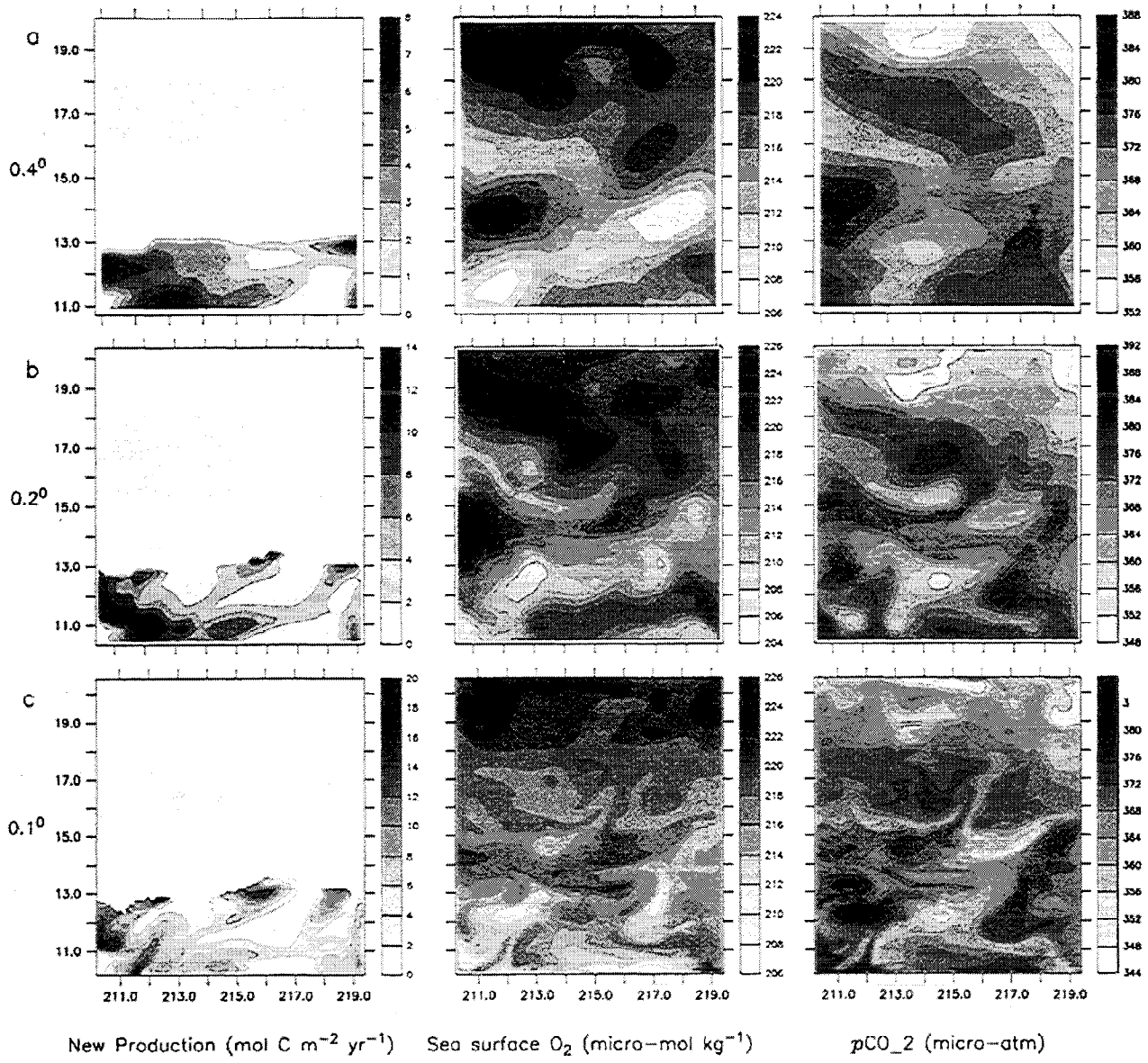

Figure 3b. Same as Figure 3a but for new production (moles carbon $m^{-2}yr^{-1}$), O_2 (μmol kg^{-1}), and pCO_2 (μatm).

3–4 moles carbon m^{-2} yr^{-1} in the Sargasso Sea near Bermuda. In the Hawaii region we predict values of new production that are in the range of 2.5–3.5 moles carbon m^{-2} yr^{-1} in the postsummer period. Values of production measured at the HOT station [*Emerson et al.*, 1997] are in the range of 2 moles carbon m^{-2} yr^{-1} and vary significantly with time [*Karl et al.*, 1996; *Winn et al.*, 1993]. The model is by no means an accurate representation of the ocean at a particular time and the values of new production predicted by the very simple biological model are highly dependent on the initial nutrient distribution and the SC-driven flow field in the domain. It demonstrates, nonetheless, that much higher values of new production can be predicted when higher resolution is used to capture the processes that supply nutrient to the euphotic zone.

The nitrate fluxes and new production diagnosed by the model could clearly not be supported by small scale mixing. A vertical eddy diffusivity of 1.3–2.3 cm^2 s^{-1} acting on the initial nitrate profile would be required across the base of the cuphotic zone (160 m) near Bermuda to support the levels of production (2.2–3.6 moles carbon m^{-2} yr^{-1}) diagnosed there by the model. Since the initial nutrient profile is set to have zero nutrient in the euphotic zone, initial gradients are artificially high. At later times an even higher eddy diffusivity would be required to maintain the same nutrient flux.

Several lines of evidence suggest that vertical motion is considerably enhanced at fronts and that water is upwelled to the surface layer or subducted from it along sloping isopycnal surfaces that may outcrop into it. Fronts and mesoscale jets that are often associated

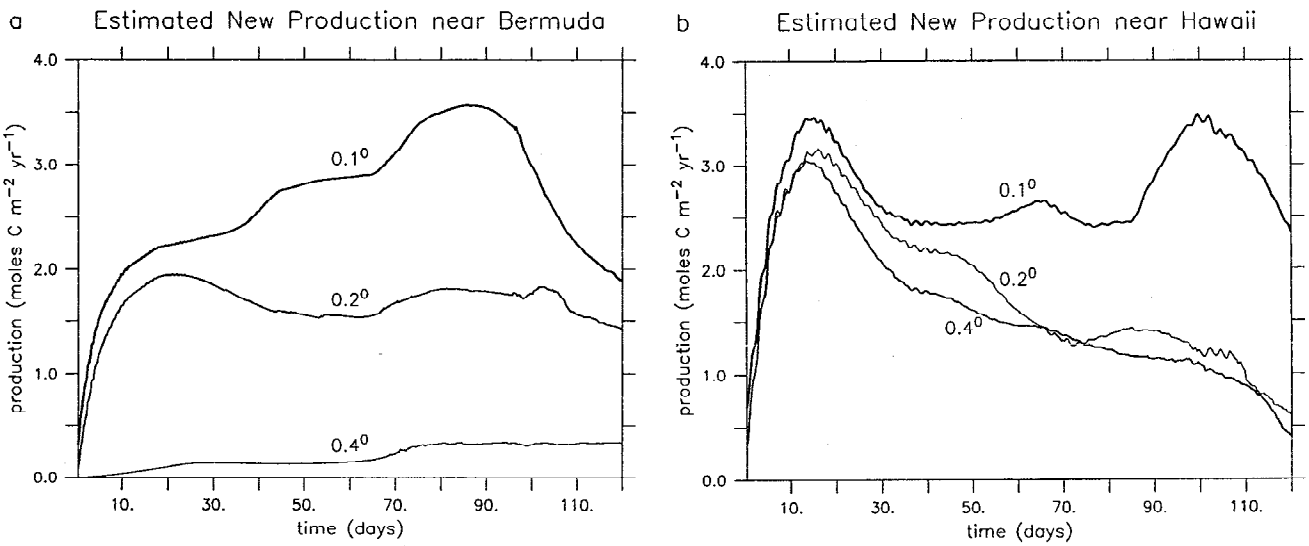

Figure 4. New phytoplankton production rate averaged over the area of the domain for the three different resolution model runs from August through November 1987 at (a) Bermuda and (b) Hawaii. The model is initialized with no nutrient in the euphotic zone and permits no horizontal flux of nutrient into the euphotic zone either. In general (except for the 0.2° and 0.4° curves at Hawaii, which are not significantly different,), the higher resolution model runs show higher levels of new production. We have used the middle 80 days of the model run (based on *Mahadevan and Archer*, [1998, Figure 5]) average values of production for the region. The flow takes some time to spin up, especially on the finer grid for which coarse initial conditions are used, and begins to show some deterioration toward the end of the model run because of the growing mismatch between the model's interior and forcing boundary conditions.

Table 1. Model and Field Estimates of New Production Rates (moles carbon m^{-2} yr^{-1})

Near Bermuda	
Using $K_z = 0.1^a$cm^{2}s^{-1} on the mean nutrient profile	0.15
0.4° resolution model	0.2–0.33
0.2° resolution model	1.6–1.9
0.1° resolution model	2.0–3.6
Based on ^{14}C [*Platt and Harrison*, 1985]	2.1 ±0.58
From sediment traps [*Lohrenz*, 1992]	0.78
From sediment traps [*Altabet*, 1989]	2.8
From OUR at Stn S [*Jenkins and Goldman*, 1985]	4.17
Based on He [*Jenkins*, 1988]	3.7
From O_2 concentrations (using 0:C -176:140) [*Spitzer and Jenkins*, 1989]	4.4 ± 1.2
From OUR estimates based on ^{3}He inventories [*Sarmiento et al.*, 1990]	3.36 ± 1.8
Near Hawaii	
0.4° resolution model	0.75–3.1
0.2° resolution model	0.75–3.1
0.1° resolution model	2.5–3.5
From sediment traps [*Karl et al.*, 1996]	0.88
From on ^{13}C/^{12}C and DIC [*Quay and Anderson*, 1996]	1 ± 0.5
Based on proteins [*Laws*, 1991]	2.5
Mass balances [*Emerson et al.*, 1997]:	
dissolved oxygen	2.7 ± 1.7
inorganic carbon	1.6 ± 0.9
organic carbon	2.0 ± 0.9

In our model, new production is inferred from the vertical flux of nutrients into the euphotic zone. Model rates presented here are the range of average values for the region, neglecting the first few days after initializing the euphotic zone with zero nutrient. The model values are representative of the postsummer period when production is low. OUR is oxygen utilization rate; and DIC is dissolved inorganic carbon.

[a]The value of the vertical mixing coefficient K_z is chosen to represent observed values [*Ledwell et al.*, 1993].

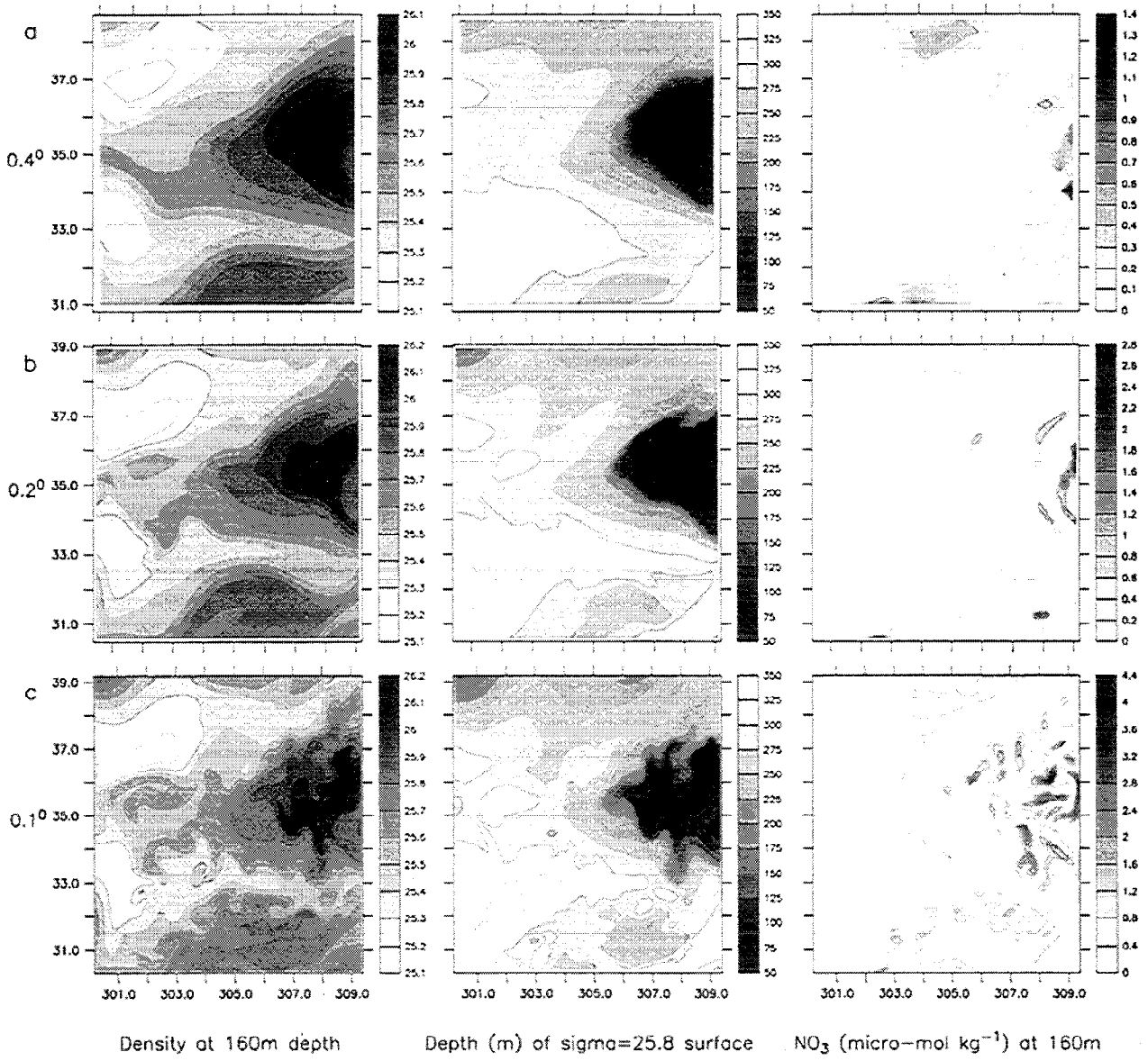

Figure 5a. Results for the Bermuda site. The density and nitrate distribution plotted at the base of the euphotic zone alongside the depth of a particular isopycnal surface. In each column we show fields from the (a) 0.4°, (b) 0.2°, and (c) 0.1° model resolutions. The nitrate distribution at the base of the euphotic zone is very similar to the pattern of new production that results from its being fluxed upward (see Figures 2 and 3). New production is concentrated in regions where the nutrient-rich isopycnals outcrop into the euphotic zone. Increasing the model resolution results in more undulation of the isopycnal surfaces and an increased length of the frontal zone or isopycnal outcropping.

with them are ubiquitous to the surface ocean. The mesoscale jets have a steeply sloping isopycnal structure in the cross-flow direction on account of geostrophic balance. They are unstable and meander, sometimes forming eddies. In the simulations, fronts are not only intensified with increasing resolution, but the length of the frontal zone is also considerably increased. Our high-resolution model results are consistent with observations of fronts made by *Voorhis and Bruce* [1982] and later by *Pollard and Regier* [1992] during the Frontal Air-Sea Interaction Experiment (FASINEX) survey in the Sargasso Sea near Bermuda. These include straining of the surface temperature field into elongated (100 km) tongues of alternating warm and cold water with vertical velocities of 30–50 m day^{-1} and the largest vertical velocity occurring at ~200 m depth. When we qualitatively compare the modeled nutrient uptake or new production (Figures 2 and 3) which is indicative of upwelling, with a plot by *Rudnick* [1996] that shows positive vertical velocities computed from the omega equation, the size and distribution of the upwelling regions look comparable. These observational data are

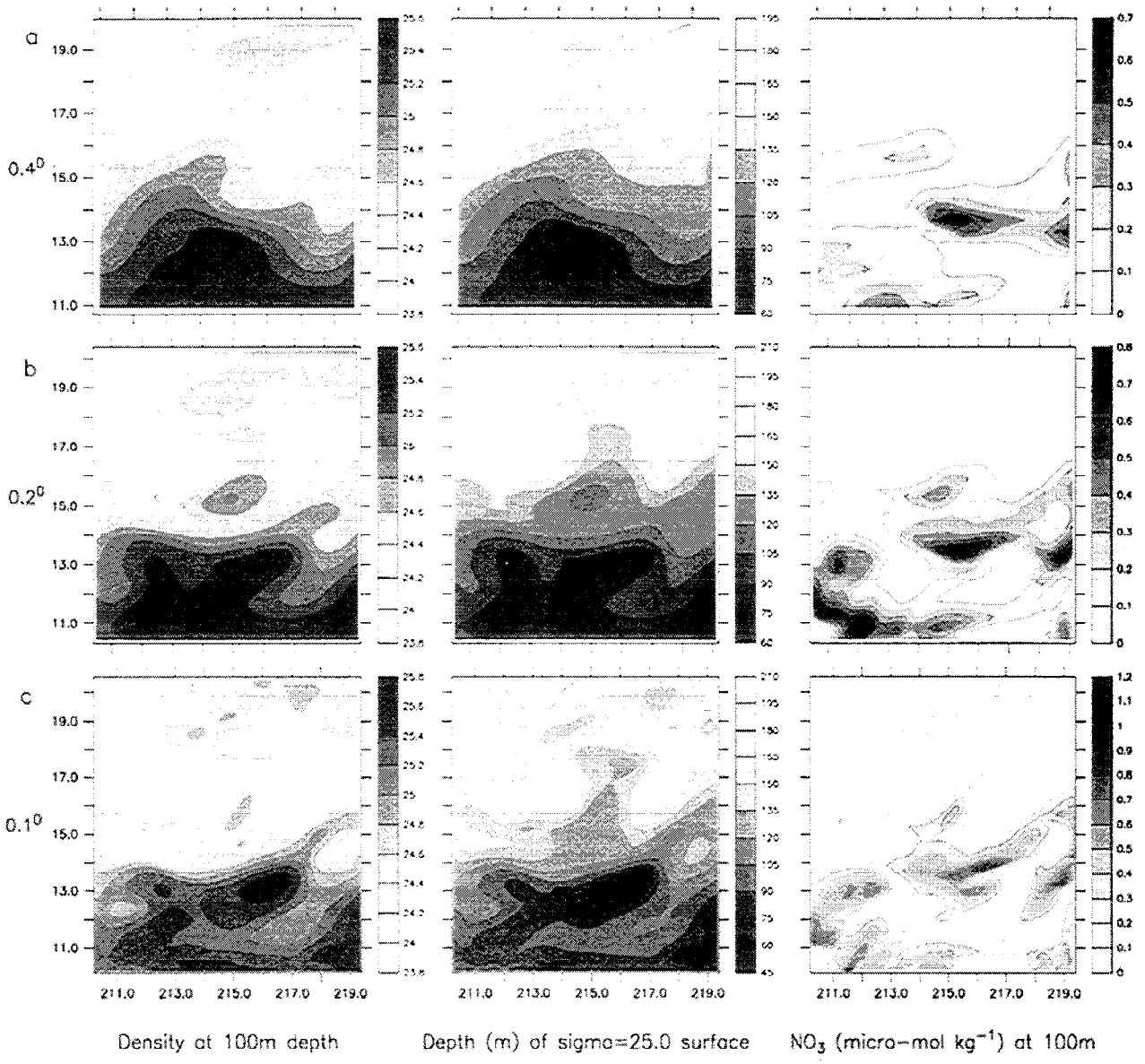

Figure 5b. Same as Figure 5a but for the Hawaii site.

at a resolution of 3.5 km along the ship track but at a spacing of 25 km in the other direction. Small-scale (10–20 km) variations in the potential vorticity plotted by *Pollard and Regier* [1990] in the much more finely resolved along-track direction (the sea soar completes a cycle every 3 km) indicate that variations in vertical velocity may occur on a similar 10–20 km scale to facilitate the conservation of potential vorticity by fluid parcels. A grid spacing of 2.5–5 km would be required to resolve this fine-scale structure.

In Figure 5 we plot snapshots of the density field and nutrient availability at the base of the euphotic zone, alongside the depth of an isopycnal surface for different model resolutions at Bermuda and Hawaii. The intense patches of biological activity (new production) in the model (Figures 2 and 3) match the patches of high nitrate concentration (Figure 5) and are focussed in regions where denser isopycnals carrying nutrient-rich subsurface water outcrop at the base of the euphotic zone. At higher resolution the isopycnal surfaces rise and fall more abruptly, fronts are more developed, horizontal gradients are stronger and vertical motion is enhanced. Once subsurface water is brought to the near surface isopycnally (this is pronounced along fronts), it is mixed across isopycnals much more easily by horizontal motion and wind-induced stirring of the surface layer. Nutrient supply to the euphotic zone is dependent on the ambient nutrient distribution and the density structure and flow field that control the vertical motion. Internal waves that cause a heaving of isopycnals make almost no contribution to the biological production since their timescale is shorter than what is required by the biology to convert nutrient to organic matter.

The eddy-pumping mechanism of nutrient supply described by *McGillicuddy and Robinson* [1997] and *McGillicuddy et al.* [1998] is not inconsistent with the more generalized frontal mechanism described here. Eddies may be viewed as circular fronts. While their doming isopycnals provide a pathway for subsurface nutrients, substantial nutrient transport can occur even in their absence as is evidenced by the enhanced supply of nutrients seen at outcropping isopycnals in this model. Since a quasigeostrophic model [*McGillicuddy and Robinson*, 1997] does not produce the same complexity of the flow field and frontal structure as a fully three-dimensional model, we believe that the latter does a much better job of simulating the vertical transport mechanisms in the ocean.

The model results show, like observations, that rates of new production are highly variable in time and space. Small localized regions of strong upwelling can support rates of new production as high as 60–80 moles carbon m^{-2} yr^{-1} in small patches for a few days at a time (Figures 2 and 3). Over a larger region these production rates average out to the values presented above and in Figure 4. Increased model resolution results in an increased variance in the new production rate over the region, indicating that upwelling is intensified at higher resolution on account of better resolved gradi-

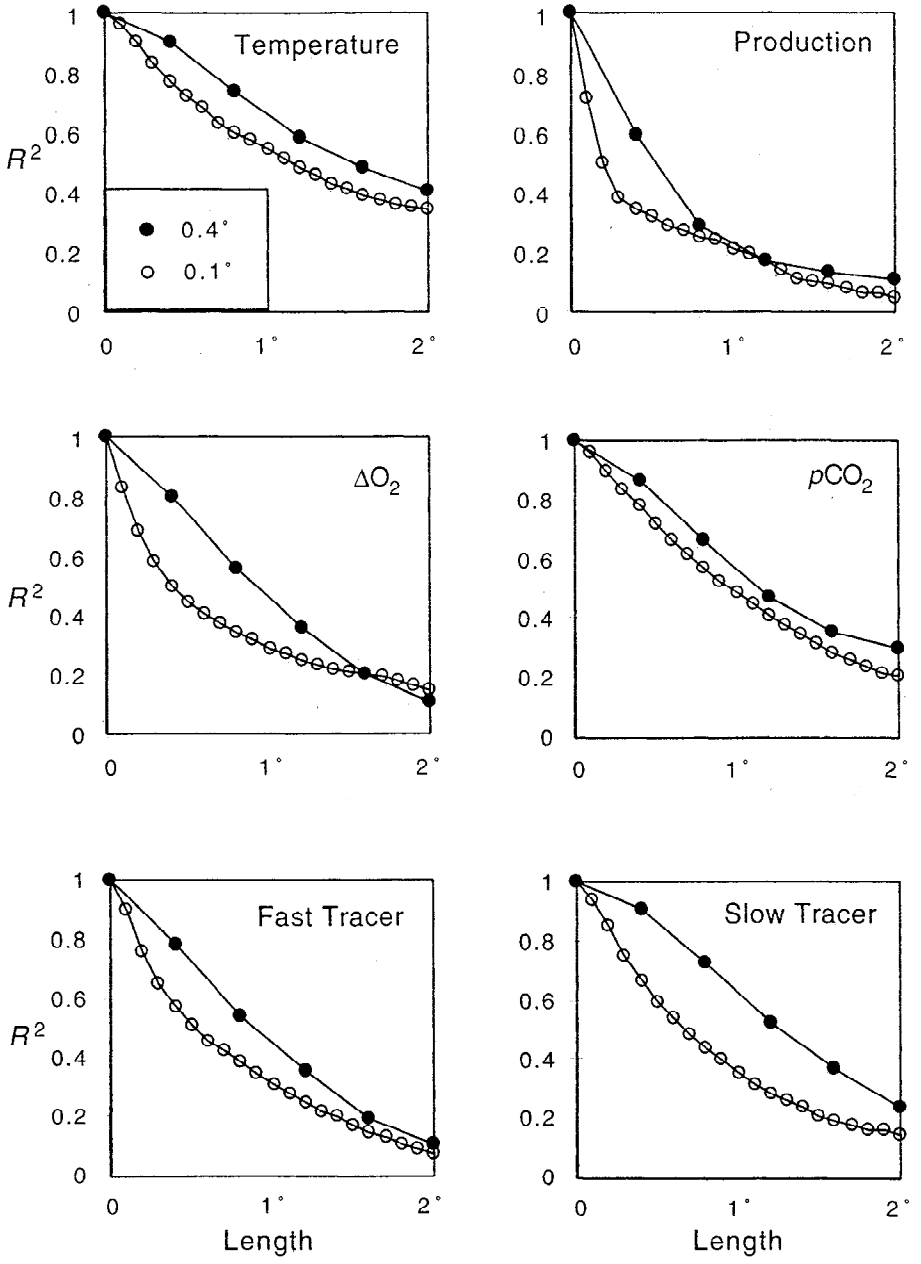

Figure 6. The correlation coefficient (defined in (10)) plotted for various sea surface properties for the 0.4°- (closed circles) and 0.1°- (open circles) resolution models.

ents. Since the scale corresponding to the thickness of fronts is typically even smaller than the internal Rossby radius of deformation, the patches of vertical velocity, biological production, and near-surface nutrient are also correspondingly fine-scaled.

In order to diagnose the characteristic length scales of the various geochemical tracer distributions we plot the correlation coefficient

$$R = \Sigma[c'(x)c'(x + \Delta x)]/\Sigma[c'(x)^2], \qquad (10)$$

where c' is the deviation of the property from its mean value, for the different tracers (Figure 6). From a perfect $R = 1$ at $\Delta x = 0$ we see a decrease in correlation with distance. New production, O_2, and the H_2O_2-like fast tracer show smaller correlation length scales than the temperature, pCO_2, and slow ventilation tracer. New production is the most anomalous of the tracers, with the smallest correlation length scale. The steep decline in correlation even one grid point away in the 0.1° model suggests that nutrient upwelling and biological production are not resolved at coarser resolutions (as that used by *Oschlies and Garcon* [1998]) and may not be adequately resolved even at 0.1° resolution. The other tracers, pCO_2, total CO_2, alkalinity, and the DOC-like slow ventilation tracer, do not show the small-scale variability seen in the nutrient uptake, O_2, and H_2O_2-like fast tracer that respond rapidly to the vertical motion (Figures 2 and 3).

3.2. Signatures of Mesoscale Motions for Field Detection

In addition to understanding the mechanism by which mesoscale motion affects the nutrient and carbon budget of the upper ocean, we would like to assess the effect of these motions on geochemical tracers that might be measurable in the field. The mesoscale dynamics of the upper ocean can be reconstructed from a high resolution subsurface density field obtained with a seasoar [*Pollard and Regier*, 1990; *Rudnick*, 1996] and the horizontal velocity structure obtained from a ship-mounted acoustic doppler current profiler (ADCP). Vertical motions are not directly detectable using these methods but can be constructed assuming quasigeostrophy from the omega equation [*Hoskins et al.*, 1978]. Our hope is to find geochemical proxies for vertical motions that could provide an independent corroboration of the vertical motions implied by these techniques.

Typically, field measurements show a greater variability than one-dimensional upper ocean biogeochemical models [*Archer et al.*, 1993; *Doney et al.*, 1996]. Table 2 reveals, however, that there is no systematic dependence of the the sea surface variance on model resolution for most properties, the exception being nutrient uptake or new production. The variance of nitrate uptake increases significantly with model resolution. It is intriguing that this is not the case for the the other biogeochemical tracers and could mean that the biogeochemical tracers are not a very good diagnostic for the intensity of upwelling or magnitude of nutrient uptake.

The gaseous tracers pCO_2 and O_2 are both affected by biological production and by equilibration with the atmosphere. They differ primarily in the buffering effect of seawater to CO_2, which enhances the storage capacity of seawater for CO_2 and lengthens the equilibration time by roughly a factor of 10 [*Broecker and Peng*, 1982]. Two factors suggest a greater sensitivity of sea surface oxygen than pCO_2 to biological forcing. The first is a visual comparison of the snapshots (Figures 2 and 3); oxygen has a greater resemblance to nitrate uptake than does pCO_2. The second is the spatial correlation result (Figure 6), which shows smaller spatial scales for sea surface oxygen than for pCO_2, and a greater sensitivity to model resolution, as seen for the nutrient uptake distribution statistics. We conclude that one of the best indicators for vertical motions in the ocean may be simply the fine-scale variability in the sea surface oxygen distribution.

The oxygen supersaturation values from the model at Bermuda (0–5% above saturation) are considerably smaller than those measured at Bermuda by *Spitzer and*

Table 2. Statistics of Sea Surface Properties

	Bermuda				Hawaii			
	0.4°		0.1°		0.4°		0.1°	
	mean	σ	mean	σ	mean	σ	mean	σ
Nitrate uptake	0.13	0.17	0.41	0.63	0.20	0.38	0.31	0.63
Temperature	24.70	0.86	24.34	0.87	26.10	0.39	25.63	0.53
Density	1024.45	0.22	1024.53	0.21	1022.49	0.23	1022.71	0.29
AOU	2.79	3.33	2.43	3.10	-0.92	3.67	-0.88	1.91
TCO_2	2035.61	11.19	2040.86	11.49	1973.07	2.00	1975.22	3.64
Alkalinity	2378.69	12.97	2383.94	8.73	2299.16	2.98	2300.94	3.04
pCO_2	368.60	15.26	364.44	17.66	370.35	4.36	365.48	6.11
Fast tracer	0.92	0.04	0.91	0.04	0.87	0.04	0.86	0.04
Slow tracer	0.84	0.08	0.82	0.06	0.88	0.05	0.85	0.06

Here σ is the standard deviation; AOU is apparent oxygen utilization; and TCO_2 is total CO_2.

Jenkins [1989] (generally, 10–15% above saturation during the summer months). In part, this can be explained by the lower net carbon export production predicted in the model. (It is roughly 35% of the *Spitzer and Jenkins* [1989] predicted values, which were supported by a high rate of vertical mixing $\sim 0.9 \times 10^{-4}$ m^2 s^{-1}.) Some of the discrepancy may be due to the seasonal temperature cycle of the upper ocean. Its contribution to oxygen supersaturation is expected to be roughly equal to the 3% summer supersaturation of argon observed in the field. While our regional model does account for sea surface warming, it is initialized with saturation values of oxygen, thus probably negating much of the contribution of seasonal warming to summertime oxygen values. Finally, the mesoscale model neglects the effects of bubble injection, which would tend to offset both the oxygen and the argon toward higher steady state sea surface concentrations.

The two tracers of sea surface exposure time, similar in their dynamics to DOC and H_2O_2, tell a similar story (Figures 2 and 3). In our simple model formulation, there is no explicit link to biological activity, and the tracers respond directly to vertical displacement due to fluid flow. The faster equilibration timescale tracer has a closer link to the same vertical motions that drive biological activity. The spatial scale of the fast tracer is somewhat smaller than the spatial scale for the slow sea surface exposure tracer, but the distinction is not as dramatic as it is between pCO_2 and O_2. The model results suggest that high-resolution surface or subsurface measurements of H_2O_2 might be useful for discerning regions of recent vertical motion and associated biological activity if the variations in H_2O_2 are not, in reality, obscured by other factors.

It seems then that nutrients, O_2, and the H_2O_2-like tracer, which are closely tied to the vertical motion of the fluid, show variations on smaller scales than do tracers that are affected by the horizontal motion. The implication is that vertical motion occurs on small scales, and the exchange of subsurface water with the surface takes place during events when sloping subsurface isopycnals outcrop at the base of the euphotic zone. Such isopycnal transport is greatly enhanced in fronts and eddies. They need to be resolved in order to capture the biological response and the distribution of properties that respond on short timescales to the vertical motion.

4. Conclusions

We find that in the pelagic ocean the vertical transport of nutrient-rich waters to the euphotic zone takes place predominantly at mesoscales and frontal scales along isopycnals. It is therefore necessary to resolve the mesoscale and possibly even the frontal scale in order to fully capture the nutrient transport and resulting biological production. The vertical motion associated with the straining and deformation of the flow field and with eddies and fronts is highly underrepresented in coarse-resolution ocean models. It is an important mechanism for nutrient supply that is missing in large-scale biogeochemical models of the ocean and could account for much of the observed new production in the oligotrophic subtropical gyres.

The sea surface variability of all properties shows a marked increase when the internal Rossby radius of deformation is resolved. However, there are indications that tracers and processes that respond rapidly to the vertical motion vary on yet smaller scales corresponding to the width of fronts. Tracers such as pCO_2 and alkalinity that are not as closely tied to the vertical velocity vary on a slightly larger scale (the mesoscale) than that of the nutrient uptake. Sea surface oxygen seems to be an excellent indicator of new production.

Finally, we should keep in mind that the large-scale isopycnal structure of the ocean and its underlying nutrient distribution are important in determining the nature of the small-scale upwelling events through which the bulk of nutrient supply to the subtropical gyres takes place. Hence small changes in the large-scale structure over climatic timescales could lead to substantial changes in the chemistry and biological productivity of the ocean basins.

Acknowledgments. We are grateful to A.J. Semtner for making the 1/4° SC model output available to us.

References

Altabet, M., Particulate new nitrogen fluxes in the Sargasso Sea, *J. Geophys. Res., 94*, 12,771–12,779, 1989.

Archer, D., S. Emerson, T. Powell, and C. Wong, Numerical hindcasting of sea surface PCO_2 at Weathership Station Papa, *Prog. in Oceanogr., 32*, 319–351, 1993.

Archer, D., E. Peltzer, and D. Kirchman, A timescale for dissolved organic carbon production in equatorial Pacific surface waters, *Global Biogeochem. Cycles, 11*, 435–452, 1997.

Bacastow, R., and E. Maier-Reimer, Dissolved organic carbon in modeling oceanic new production, *Global Biogeochem. Cycles, 5*, 71–86, 1991.

Bleck, R., R. Onken, and J. Woods, A two-dimensional model of mesoscale frontogenesis in the ocean, *Q. J. R. Meteorol. Soc., 114*, 347–371, 1988.

Broecker, W. S., and T.-H. Peng, *Tracers in the Sea*, Lamont-Doherty Geol. Obs., Columbia Univ., Palisades, N.Y., 1982.

Buesseler, K., Do upper-ocean sediment traps provide an accurate record of particle flux?, *Nature, 353*, 420–423, 1991.

Caldwell, D., Small-scale physics of the ocean, *Rev. Geophys., 21*, 1192–1205, 1983.

Carlson, C., H. Ducklow, and A. Michaels, Annual flux of dissolved organic carbon from the euphotic zone in the northwestern Sargasso Sea, *Nature, 371*, 405–408, 1994.

Chen, D., and L. M. Rothstein, A hybrid vertical mixing scheme and its application to tropical ocean models, *J. Phys. Oceanogr., 24*, 2156–2179, 1994.

Doney, S., D. Glover, and R. Najjar, A new coupled, one-dimensional biological-physical model for the upper ocean: Applications to the JGOFS Bermuda Atlantic Time-series Study (BATS) site, *Deep Sea Res., Part II, 43*, 591–624, 1996.

Emerson, S., and T. Hayward, Chemical tracers of biological processes in shallow waters of the North Pacific preformed nitrogen distributions, *J. Mar. Res., 53*, 1–15, 1995.

Emerson, S., P. Quay, C. Stump, D. Wilbur, and M. Knox, O_2, Ar, N_2, and ^{222}Rn in surface waters of the Subarctic Ocean: Net biological O_2 production, *Global Biogeochem. Cycles, 5*, 49–71, 1991.

Emerson, S., P. Quay, D. Karl, C. Winn, L. Tupas, and M. Landry, Experimental determination of the organic carbon flux from open-ocean surface waters, *Nature, 389*, 951–954, 1997.

Eppley, R. W., and B. J. Peterson, Particulate organic matter flux and new production in the deep ocean, *Nature, 282*, 677–680, 1979.

Falkowski, P., D. Ziemann, Z. Kolber, and P. Bienfang, Role of eddy pumping in enhancing primary production in the ocean, *Nature, 352*, 55–58, 1991.

Hellerman, S., and M. Rosenstein, Normal monthly wind stress over the world ocean with error estimates, *J. Phys. Oceanogr., 13*, 1093–1104, 1983.

Hoskins, B. J., and F. P. Bretherton, Atmospheric frontogenesis models: Mathematical formulation and solution, *J. Atmos. Sci., 29*, 11–37, 1972.

Hoskins, B., I. Draghici, and H.C. Davies, A new look at the ω-equation, *Q. J. R. Meteorol. Soc., 104*, 31–38, 1978.

Jenkins, W., Nitrate flux into the euphotic zone near Bermuda, *Nature, 331*, 521–523, 1988.

Jenkins, W., and J. Goldman, Seasonal oxygen cycling and primary production in the Sargasso Sea, *J. Mar. Res., 43*, 465–491, 1985.

Johnson, K., S. Willason, D. Wiesenburg, S. Lohrenz, and R. Arnone, Hydrogen peroxide in the western Mediterranean Sea: A tracer for vertical advection, *Deep Sea Res., Part A, 36*, 241–254, 1989.

Karl, D., J. Christian, J. Dore, R. Hebel, L. M. Tupas, and C. Winn, Seasonal and interannual variability in primary production and particle flux at station ALOHA, *Deep Sea Res., Part II, 43*, 539–569, 1996.

Laws, E., Photosynthetic quotients, new production and net community production in the open ocean, *Deep Sea Res., Part A, 38*, 143–167, 1991.

Ledwell, J., A. Wilson, and C. Low, Evidence for slow mixing across the pycnocline from an open-ocean tracer-release experiment, *Nature, 364*, 701–703, 1993.

Levitus, S., Climatological atlas of the world ocean, *NOAA Prof. Pap. 13*, 173, 1982.

Lewis, M., W. Harrison, N. Oakey, D. Hebert, and T. Platt, Vertical nitrate fluxes in the oligotrophic ocean, *Science, 234*, 870–873, 1986.

Lohrenz, S., Seasonal variability in primary production and particle flux in the northwestern Sargasso Sea: U.S. JGOFS Bermuda Atlantic Time-series Study, *Deep Sea Res., Part A, 39*, 1373–1391, 1992.

Lyman, J., Buffer mechanism of sea water, Ph.D. thesis, Univ. of Calif., Los Angeles, 1956.

Mahadevan, A., and D. Archer, Modeling a limited region of the ocean, *J. Comput. Phys., 145*, 555–574, 1998.

Maier-Reimer, E., Geochemical cycles in an ocean general circulation model, *Global Biogeochem. Cycles, 7*, 645–678, 1993.

Martin, J., G. Knauer, D. Karl, and W. Broenkow, VERTEX: Carbon cycling in the northeast Pacific, *Deep Sea Res., Part A, 34*, 267–285, 1987.

McClean, J., and A. Semtner, Comparisons of mesoscale variability in the Semtner-Chervin 1/4° model, the Los Alamos parallel ocean program 1/6° model, and TOPEX/Poseidon data, *J. Geophys. Res., 102*, 25, 203–25, 226, 1997.

McGillicuddy, D., Jr., and A. Robinson, Eddy induced nutrient supply and new production in the Sargasso Sea, *Deep Sea Res., Part I, 44*, 1427–1450, 1997.

McGillicuddy, D., Jr., A. Robinson, D. Siegel, H. Jannasch, R. Johnson, T. Dickey, J. McNeil, A. Michaels, and A. Knap, Influence of mesoscale eddies on new production in the Sargasso Sea, *Nature, 394*, 263–266, 1998.

Mehrbach, C., C. Culberson, J. Hawley, and P. Pytkowicz, Measurement of the apparent dissociation constants of carbonic acid in seawater at atmospheric pressure, *Limnol. and Oceanogr., 18*, 897–907, 1973.

Michaels, A., N. Bates, K. Buesseler, C. Carlson, and A. Knap, Carbon-cycle imbalances in the Sargasso Sea, *Nature, 372*, 537 540, 1994a.

Michaels, A., A. Knap, R. Dow, K. Gunersen, R. Johnson, J. Sorensen, A. Close, and G. Knaueret, Seasonal patterns of ocean biogeochemistry at the U.S. JGOFS Bermuda Atlantic Time-series Study site, *Deep Sea Res., 41*, 1013–1039, 1994b.

Najjar, R., Simulations of the phosphorus and oxygen cycles in the world ocean using a general circulation model, Ph.D. thesis, Princeton Univ., Princeton, N.J., 1990.

Najjar, R., J. Sarmiento, and J. Toggweiler, Downward transport and fate of organic matter in the ocean: Simulations with a general circulation model, *Global Biogeochem. Cycles, 6*, 45–76, 1992.

Oschlies, A., and V. Garcon, Eddy-induced enhancement of primary production in a model of the North Atlantic Ocean, *Nature, 394*, 266–269, 1998.

Platt, T., and W. G. Harrison, Biogenic fluxes of carbon and oxygen in the ocean, *Nature, 318*, 55–58, 1985.

Pollard, R., and L. Regier, Large variations in potential vorticity at small spatial scales in the upper ocean, *Nature, 348*, 227–229, 1990.

Pollard, R., and L. Regier, Vorticity and vertical circulation at an ocean front, *J. Phys. Oceanogr., 22*, 609–625, 1992.

Quay, P., and H. Anderson, Organic carbon export rates in the subtropical N. Pacific, *Eos Trans. AGU, 77*(3), *Ocean Sci. Meet. Suppl.,*, OS85, 1996.

Rudnick, D. L., Intensive surveys of the Azores front. Part II: Inferring the geostrophic and vertical velocity fields, *J. Geophys. Res., 101*, 16,291–16,303, 1996.

Sarmiento, J., G. Thiele, R.M. Key, and W. Moore, Oxygen and nitrate new production and remineralization in the North Atlantic subtropical gyre, *J. Geophys. Res., 95*, 18,303–18,315, 1990.

Sarmiento, J., R. Slater, M. Fasham, H. Ducklow, J. Toggweiler, and G. Evans, A seasonal three-dimensional ecosystem model of nitrogen cycling in the North Atlantic euphotic zone, *Global Biogeochem. Cycles, 7*, 417–450, 1993.

Sathyendranath, S., T. Platt, E. Horne, W. Harrison, O. Ulloa, R. Outerbridge, and N. Hoepffner, Estimation of new production in the ocean by compound remote sensing, *Nature, 353*, 129–133, 1991.

Semtner, A.J., Jr., and R. Chervin, Ocean general circulation from a global eddy-resolving model, *J. Geophys. Res., 97*, 5493–5550, 1992.

Shearman, R.K., J.A. Barth, and P.M. Kosro, Diagnosis of three-dimensional circulation associated with mesoscale motion in the California current, *J. Phys. Oceanogr., 29*, 651–670, 1999.

Spall, M. A., Frontogenisis, subduction, and cross-front exchange at upper ocean fronts, *J. Geophys. Res., 100*, 2543–2557, 1995.

Spitzer, W., and W. Jenkins, Rates of vertical mixing, gas exchange, and new production estimates from seasonal gas cycles in the upper ocean near Bermuda, *J. Mar. Res., 47*, 169–196, 1989.

Stammer, D., R. Tokmakian, and C. Wunsch, How well does a 1/4° global circulation model simulate large-scale

oceanic observations, *J. Geophys. Res., 101*, 25,779–25,811, 1996.

Takahashi, T., W. Broecker, and S. Langer, Redfield ratio based on chemical data from isopycnal surfaces, *J. Geophys. Res., 90*, 6907–6924, 1985.

Voorhis, A., and J. Bruce, Small-scale surface stirring and frontogenesis in the subtropical convergence of the western North Atlantic, *J. Mar. Res., 40*, suppl., 801–821, 1982.

Williams, R. G., and M. J. Follows, The Ekman transfer of nutrients and maintenance of new production over the North Atlantic, *Deep Sea Res., Part I, 45*, 461–489, 1998.

Winn, C., R. Lukas, D. Karl, and E. Firing, Hawaii Oceanographic Time-series Program, *Tech Rep. 93-3*, School of Ocean and Earth Sci. and Technolo., Univ. of Hawaii at Manoa, Honolulu, 1993.

A. Mahadevan, Atmospheric and Environmental Research, 840 Memorial Drive, Cambridge, MA 02139. (amala@aer.com)

D. Archer, Department of Geophysical Sciences, University of Chicago, 5734 S. Ellis Av., Chicago, IL 60637. (archer@starbuck.uchicago.edu)

(Received November 5, 1998; revised June 10, 1999; accepted July 1, 1999.)